

# Learning More with Less: A Generalizable, Self-Supervised Framework for Privacy-Preserving Capacity Estimation with EV Charging Data

Anushiya Arunan

Engineering Product Development  
Singapore University of Technology and Design  
Email: anushiya\_arunan@mymail.sutd.edu.sg

Yan Qin

School of Automation  
Chongqing University  
Email: yan.qin@cqu.edu.cn

Xiaoli Li

Information Systems Technology and Design  
Singapore University of Technology and Design  
Email: xiaoli\_li@sutd.edu.sg

U-Xuan Tan

Engineering Product Development  
Singapore University of Technology and Design  
Email: uxuan\_tan@sutd.edu.sg

H. Vincent Poor

Electrical and Computer Engineering  
Princeton University  
Email: poor@princeton.edu

Chau Yuen

Electrical and Electronics Engineering  
Nanyang Technological University  
Email: chau.yuen@ntu.edu.sg

**Abstract**—Accurate battery capacity estimation is key to alleviating consumer concerns about battery performance and reliability of electric vehicles (EVs). However, practical data limitations imposed by stringent privacy regulations and labeled data shortages hamper the development of generalizable capacity estimation models that remain robust to real-world data distribution shifts. While self-supervised learning can leverage unlabeled data, existing techniques are not particularly designed to learn effectively from challenging field data—let alone from privacy-friendly data, which are often less feature-rich and noisier. In this work, we propose a first-of-its-kind capacity estimation model based on self-supervised pre-training, developed on a large-scale dataset of privacy-friendly charging data snippets from real-world EV operations. Our pre-training framework, *snippet similarity-weighted masked input reconstruction*, is designed to learn rich, generalizable representations even from less feature-rich and fragmented privacy-friendly data. Our key innovation lies in harnessing contrastive learning to first capture high-level similarities among fragmented snippets that otherwise lack meaningful context. With our snippet-wise contrastive learning and subsequent similarity-weighted masked reconstruction, we are able to learn rich representations of both granular charging patterns within individual snippets and high-level associative relationships across different snippets. Bolstered by this rich representation learning, our model consistently outperforms state-of-the-art baselines, achieving 31.9% lower test error than the best-performing benchmark, even under challenging domain-shifted settings affected by both manufacturer and age-induced distribution shifts.

**Index Terms**—Battery capacity estimation, self-supervised learning, contrastive learning, data privacy, electric vehicles.

## I. INTRODUCTION

Electric vehicles (EVs), powered by lithium-ion batteries, possess the transformative potential to accelerate the decarbonization of the transportation sector [1]. However, consumer concerns, such as uncertainties about driving range, long charging times, and battery safety, present significant barriers to the widespread adoption of EVs over their fossil fuel-based counterparts [2]. A key to alleviating these concerns is the availability of accurate battery capacity estimation—which serves as the foundation for making informed and optimal decisions about journey planning and battery maintenance [3].

Batteries gradually lose capacity over time, with the deterioration influenced by a combination of factors such as the intensity of charge-discharge cycles [4] and operating environments [5]. As a result, accurately estimating battery capacity is highly challenging, especially under real-world conditions outside of controlled laboratory settings. Machine learning—especially deep learning (DL)—provides a flexible approach for capturing the complex dependencies affecting capacity degradation. By leveraging data mining and pattern analysis, DL models can bypass the need for detailed mechanistic modeling to learn generalizable features [6], [7]. In recent years, DL techniques have become indispensable for the battery research community, driven by the growth in benchmark battery datasets and architectural advancements in

time series modeling [8], [9].

However, training data from actual EV operations is often scarce in practice due to two critical constraints. First, as regulatory scrutiny over responsible artificial intelligence increases, data security and privacy laws are poised to become more stringent globally [10]–[12]. From the seminal General Data Protection Regulation to the newly proposed EU Artificial Intelligence Act [13], regulations increasingly mandate user consent and minimization of collected data—which limit EV manufacturers’ ability to curate rich training data from real-world driving operations [14]. Second, even when battery data is available, parsing complex sensor readings and annotating them with ground-truth capacity labels is a resource-intensive endeavor requiring specialized domain expertise [3]. With recent advancements like fast-charging batteries further complicating the analysis of battery behaviors [15] and raising data parsing costs, it is often only economically feasible to label a small portion of collected data [16]. In these data-scarce environments, a continued reliance on labeled data alone for model training will result in overfitted models of little practical applicability, struggling to generalize beyond the limited number of training examples [9], [17], [18].

Therefore, we posit that, for capacity estimation models to be effective under real-world data constraints, they must possess the following essential capabilities:

1. Achieve accurate capacity estimation even with privacy-friendly field data, which have significantly lower feature-richness and contextual information [3] than laboratory-generated experimental data;
2. Leverage the untapped potential of unlabeled data, which is more readily available and offers a greater diversity of training examples than small labeled datasets.

However, the few battery studies from actual EV operations tend to fall short of these requirements. Typically focused on public transportation fleets rather than private vehicles, studies often rely on detailed, privacy-sensitive operational data such as on-road driving behaviors and mileage traveled [19]–[23] to supplement battery data and achieve accurate battery health prognostics. With growing data-privacy regulations, the granular operational data needed by existing prognostics models [19]–[23] is less likely to be available, especially from private EV owners. Moreover, the dependence on supervised learning and labeled data [19]–[27] imposes a practical limit on the generalization capabilities of these models, as it is not sustainable to pre-emptively create extensive, labeled training datasets for every possible test condition.

A promising paradigm for learning generalizable models under labeled data scarcity is *self-supervised* pre-training followed by supervised fine-tuning [28]. Known for its success in computer vision, self-supervised pre-training involves solving auxiliary tasks—such as reconstructing masked out patches in images [29] or contrastive learning of image similarities [30]—to learn generalized representations and patterns of the input data, without requiring any target labels. In particular, contrastive learning has proven capable of extracting discrim-

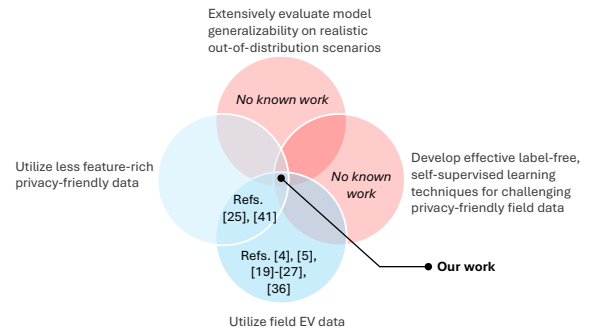


Fig. 1. Contribution of our work to the domain of practical EV battery capacity estimation using field data.

inative features, even from noisy or incomplete data [31]. By learning effectively from unlabeled data, the pre-trained model can be fine-tuned with a small amount of labeled data to adapt to any downstream task, thus reducing the massive data labeling efforts needed for fully supervised models.

Battery health prognostics stands to benefit greatly from self-supervised learning, especially given the costly domain expertise needed for data labeling. However, the few nascent efforts [32]–[34] to leverage self-supervised learning typically draw from computer vision techniques for images, and thus are not particularly well-suited to learn from time series battery measurements. For instance, some studies employ computationally intensive transformations to convert time series battery data to images [32] and adopt parameter-heavy architectures like vision transformers [32], [33] for the self-supervised representation learning. However, these approaches may not adequately capture important temporal dependencies in the battery data, resulting in a higher labeled data demand of at least 25-30% for a good fine-tuning performance downstream [9], [32], [33]. Furthermore, self-supervised learning techniques have hardly been investigated on data from actual EV operations [9], [32]–[36]—let alone on more challenging privacy-friendly data. Hence, their generalization under practical data constraints and real-world data distribution shifts are unknown.

In this work, we propose a first-of-its-kind capacity estimation model based on the self-supervised pre-training paradigm, developed and tested on a large-scale dataset of nearly 200,000 privacy-friendly, short-sequenced snippets of battery monitoring data from real-world EV charging operations (Fig. 1). Our pre-training framework, *snippet similarity-weighted masked input reconstruction*, is designed to learn rich, generalizable representations even from less feature-rich and fragmented privacy-friendly data. As a self-supervised technique, the basic principle of masked input reconstruction is to reconstruct the masked-out portions of the data as accurately as possible to the original, thereby inducing the learning of meaningful representations in the original data without any target labels. However, the higher noise-to-signal ratio in fragmented snippets of partial charging data can significantly challenge the masked reconstruction process and hamper effective representation learning.

A key innovation of our pre-training design is thus leveraging contrastive learning to learn meaningful similarity associations among the fragmented snippets, which enables the model to focus on similarities between the masked and original snippets, while suppressing noise from dissimilar snippets during the reconstruction process. Although some state-of-the-art time series pre-training frameworks [37], [38] also utilize contrastive learning, their computer vision-centric approaches (e.g., hierarchical contrastive learning or reliance on multiple masked augmentations) often introduce additional noise and complexity, which impedes optimal representation learning from already challenging field datasets. In comparison, we harness contrastive learning in a simple but impactful manner to first learn high-level similarity associations among fragmented snippets that otherwise lack meaningful context. With our snippet-wise contrastive learning and subsequent similarity-weighted masked reconstruction, we can learn rich representations of both granular charging patterns within individual snippets *and* high-level associative relationships across different snippets.

Our model’s generalizability is evaluated on a suite of diverse and challenging capacity estimation scenarios encountered by EV users and manufacturers—(i) adaptability to age-induced data distribution shifts across EV lifetime, (ii) transferability across different EV manufacturers, and (iii) robustness to novel test patterns unseen in the limited labeled fine-tuning data. Bolstered by the rich representations learnt by the pre-trained encoder, we consistently outperform existing state-of-the-art baselines [37]–[40] across these out-of-distribution scenarios, despite using only 10% labeled fine-tuning data.

Overall, the key contributions of this work are:

1. As the first generalizable capacity estimation framework developed on field EV data, our work fills an important gap in existing literature: how to learn effectively from the less feature-rich and privacy-friendly partial charging data to still yield robust and generalizable capacity estimation.
2. Our model’s generalizability extends to highly domain-shifted settings affected by both manufacturer and age-induced distribution shifts, where it still achieves 31.9% lower test error than the best-performing benchmark.
3. Departing from existing studies, our work demonstrates that developing a generalizable model does not always require extensive labeled data. This marks a pivotal step towards practically implementable capacity estimation models, amidst the dual challenges of privacy and labeled data constraints.

The rest of the paper is organized as follows. Section II establishes the data distributions for realistic out-of-distribution problem settings. Section III presents the proposed capacity estimation framework, with a focus on the self-supervised pre-training scheme. Section IV discusses the experimental results. Section V concludes and highlights future directions.

TABLE I  
OVERVIEW OF GENERATED DATA DISTRIBUTIONS

EV manufacturer	Distribution name	Accumulated mileage $m$	Short-form
EVM1	Distribution 1	$m \leq 100,000$ km	EVM1D1
	Distribution 2	$100,000 < m \leq 150,000$ km	EVM1D2
	Distribution 3	$m > 150,000$ km	EVM1D3

## II. DATA DISTRIBUTION GENERATION FOR OUT-OF-DISTRIBUTION PROBLEM DESIGN

To evaluate our capacity estimation model, we design a suite of challenging problem settings investigating diverse aspects of generalizability, including adaptability to age-induced data distribution shifts, cross-manufacturer transferability, and robustness to novel test patterns. This section establishes the data distributions for the out-of-distribution problem settings.

For the problem design, we leverage a newly released dataset of EV charging records, collected over several years from charging stations [41]. This is the largest publicly-available field data from EVs normally operating in real-world conditions. Notably, this dataset is fundamentally privacy-friendly as it contains only charging records. Battery charging data, unlike discharging data, cannot capture sensitive information on day-to-day operational behaviours [42]. Moreover, as an additional privacy-preserving measure, the raw data is already pre-segmented, and only shorter, fragmented snippets of partial charging data are provided. While this does not introduce systematic biases or diminish the dataset’s utility [41], the limited privacy-friendly features being spread across fragmented snippets makes the dataset highly challenging to work with. Nonetheless, the dataset serves as a realistic standard for the minimalistic data likely to be available under stricter privacy regulations.

The dataset contains EVs from three manufacturers, aliased as Manufacturers 1, 2, and 3. Within each manufacturer, the charging data snippets are provided at the vehicle-level. Each charging snippet only contains basic battery monitoring variables such as charging current, voltage, temperature, and state of charge, and is stored as a multivariate time series sequence. Every charging snippet has a *mileage* label indicating the EV’s accumulated mileage at the time of charging. However, only a subset of the snippets have *capacity* labels due to the complexity of the charging processes and the resource-intensive involvement of EV manufacturer engineers for capacity labeling [41].

We primarily use data from Manufacturer 1, which contains the largest number of charging snippets among the three manufacturers. We partition the charging snippets based on their mileage labels, to generate three meaningfully different data distributions, labeled 1 to 3, demarcated by the mileage thresholds shown in Table I. Fig. 2a captures the inverse relationship between the mileage and capacity labels of the charging snippets, and particularly, the capacity degradation that occurs as EVs progress from Distributions 1 to 3 over their operational lifetime. This capacity degradation results in

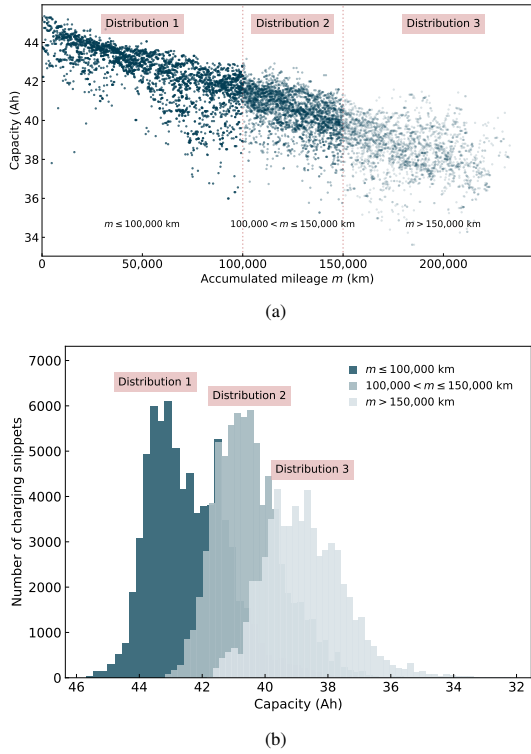


Fig. 2. Visualization of the three generated data distributions. Considering the charging snippets across all EVs, (a) illustrates the inverse relationship between the mileage and capacity labels of the charging snippets, particularly, highlighting the capacity degradation that occurs through distributions 1 to 3. (b) This capacity degradation results in the notable domain shifts.

the notable domain shifts observed among the three generated distributions (Fig. 2b), which facilitates a rigorous evaluation of our capacity estimation model’s generalizability to age-induced data distribution shifts occurring over EV lifetime.

Aside from Manufacturer 1, we also strategically leverage the smaller dataset from Manufacturer 3 to evaluate additional aspects of model generalizability, such as transferability across different EV manufacturers. To maintain brevity, we discuss this problem design together with the experimental results in later sections.

### III. PROPOSED CAPACITY ESTIMATION FRAMEWORK

We detail the capacity estimation framework, with a focus on the proposed self-supervised pre-training methodology. Fig. 3a provides an overview of the “pre-training–fine-tuning” pipeline for developing a practically effective capacity estimation model with broad generalization capabilities, even when labeled training data is limited. During pre-training, a well-designed self-supervised learning task (in our case, masked input reconstruction) trains the encoder to learn generalizable representations from the more readily available unlabeled charging snippets. During fine-tuning, a capacity estimation model for different target distributions can then be quickly trained by fine-tuning the pre-trained encoder on a small set of labeled snippets from the target distribution. The success of this transfer learning, especially with limited labeled data, hinges on the pre-training framework’s ability to learn rich,

generalizable representations that can be reused across various downstream capacity estimation scenarios.

Fig. 3b details our proposed pre-training methodology: *snippet similarity-weighted masked input reconstruction*. The basic principle of masked input reconstruction is to reconstruct the masked-out portions of time series as accurately as possible to the original, thereby inducing the learning of meaningful representations in the original time series. However, the higher noise-to-signal ratio in fragmented snippets containing only partial charging data can significantly challenge the masked reconstruction process and hamper effective representation learning. Addressing this critical gap, our pre-training method is specially designed to learn generalizable representations of broad practical applicability, even from less feature-rich and fragmented, privacy-friendly data. The key innovation lies in the snippet-wise similarity learning, which provides meaningful context to fragmented snippets. The learnt similarities are then leveraged for a similarity-weighted, point-wise reconstruction of the masked series, which significantly enhances the masked reconstruction process and, thus, the representation learning needed for the subsequent fine-tuning phase.

#### A. Self-supervised pre-training: Snippet similarity-weighted masked input reconstruction

The pre-training method comprises of four sub-components, illustrated step-by-step in Fig. 3b. We elaborate them below.

1) *Point-wise representation learning*: Given  $N$  charging snippets  $\{\mathbf{x}_i\}_{i=1}^N$ , we first generate a masked snippet  $\mathbf{x}_i^* \in \mathbb{R}^{T \times C}$  for each original snippet  $\mathbf{x}_i \in \mathbb{R}^{T \times C}$  by randomly masking a portion of the  $T$  time points for each battery monitoring variable in  $C$ . We adopt the well-established geometric masking strategy [39] to randomly mask selected temporal subsequences with zeros.

The original and masked snippets are fed into encoder  $f(\cdot)$  to learn high-dimensional representations of each time point, which we henceforth term as *point-wise representations*:

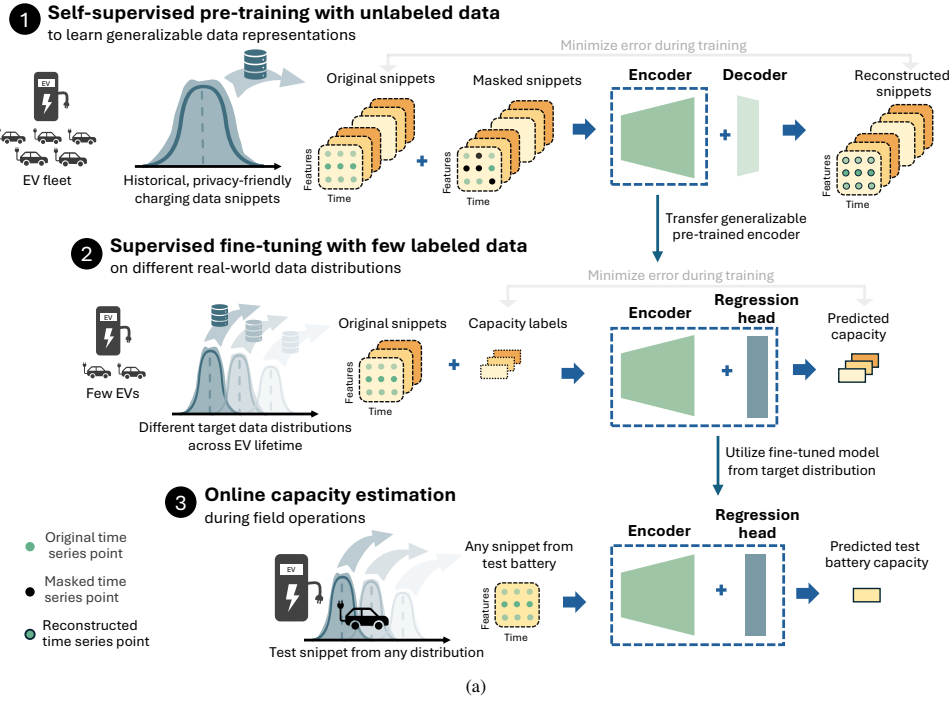
$$f\left(\bigcup_{i=1}^N (\{\mathbf{x}_i\} \cup \{\mathbf{x}_i^*\})\right) = \bigcup_{i=1}^N (\{\mathbf{p}_i\} \cup \{\mathbf{p}_i^*\}) = \mathcal{P} \quad (1)$$

where,  $\mathbf{p}_i \in \mathbb{R}^{T \times d_f}$  and  $\mathbf{p}_i^* \in \mathbb{R}^{T \times d_f}$  are point-wise representations learnt from the original and masked snippets, respectively, and  $d_f$  is the encoder’s hidden dimension. Our proposed encoder is a lightweight yet efficient, single-layer bidirectional LSTM block, designed to learn important sequential dependencies among time points in both directions.

2) *Snippet-wise representation learning*: Next, to explicitly associate the point-wise representations with their respective snippets for the downstream similarity learning, a projector  $h(\cdot)$  maps and condenses the point-wise representations into *snippet-wise representations*:

$$h\left(\bigcup_{i=1}^N (\{\mathbf{p}_i\} \cup \{\mathbf{p}_i^*\})\right) = \bigcup_{i=1}^N (\{\mathbf{s}_i\} \cup \{\mathbf{s}_i^*\}) = \mathcal{S} \quad (2)$$

where,  $\mathbf{s}_i \in \mathbb{R}^{1 \times d_h}$  and  $\mathbf{s}_i^* \in \mathbb{R}^{1 \times d_h}$  are the snippet-



### In-depth look at proposed self-supervised pre-training framework in ①: Snippet similarity-weighted masked input reconstruction

to learn rich, generalizable representations from challenging and fragmented privacy-friendly data

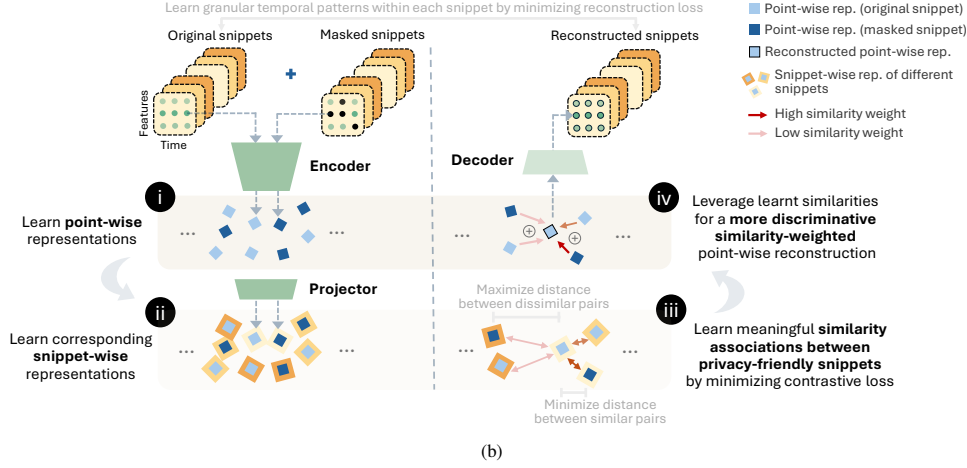


Fig. 3. (a) An overview of “pre-training–fine-tuning” pipeline for developing a generalizable capacity estimation model, followed by (b) an in-depth look at our proposed pre-training framework. The key innovation is learning meaningful similarities among the fragmented snippets, which enables the model to focus on similarities between the masked and original snippets, while suppressing noise from dissimilar snippets for the masked reconstruction process. With the snippet-wise contrastive learning and subsequent similarity-weighted masked reconstruction, the model captures rich representations of both granular charging patterns within individual snippets and high-level associative relationships across different snippets, significantly enhancing downstream capacity estimation.

wise representations learnt from the original and masked snippets, respectively,  $d_h$  is the projector’s hidden dimension. The projector is a MLP layer that aggregates the point-wise representations from all  $T$  time points in the snippet sequence into a single snippet-wise representation.

3) *Snippet-wise similarity learning*: Learning *snippet-wise similarities* is the key feature of our model design for learning effectively from fragmented and short-sequenced privacy-friendly snippets. To successfully reconstruct the original point-wise representation  $\mathbf{p}_i$  from its masked counterpart  $\mathbf{p}_i^*$ ,

the model needs to recognize that both representations originate from the same underlying snippet, and thus their snippet-wise representations  $\mathbf{s}_i$  and  $\mathbf{s}_i^*$  should have high similarity. This is especially crucial when dealing with privacy-friendly, short-sequence snippets, as their relatively higher noise-to-signal ratio can significantly challenge the reconstruction process and, ultimately, hamper the learning of meaningful representations from input snippets.

We leverage contrastive learning [30] and propose a new contrastive loss formulation to learn the pair-wise similarities

and dissimilarities among the snippet-wise representations in  $\mathcal{S}$ . The contrastive loss  $\mathcal{L}_c$  is formalized as:

$$\mathcal{L}_c = - \sum_{\mathbf{s} \in \mathcal{S}} \left( \sum_{\mathbf{s}' \in \mathcal{S}^+} \log \frac{\exp(D_{\mathbf{s}, \mathbf{s}'}/\tau)}{\sum_{\mathbf{s}'' \in \mathcal{S} \setminus \{\mathbf{s}\}} \exp(D_{\mathbf{s}, \mathbf{s}''}/\tau)} \right) \quad (3)$$

where,  $\mathbf{s}' \in \mathcal{S}^+ \subset \mathcal{S}$  are representations similar to  $\mathbf{s}$ ,  $D_{\cdot, \cdot}$  is a pairwise cosine similarity value in the similarity matrix  $\mathbf{D}$ , and  $\tau$  is the temperature parameter controlling the contrast between similar and dissimilar pairs in the softmax normalization above.

Minimizing  $\mathcal{L}_c$  requires decreasing the cosine distance between similar snippet representations from the original snippets and their masked counterparts, while increasing the distance between dissimilar snippet representations. This guides the projector  $h(\cdot)$  to learn a more discriminative snippet-wise representation space.

#### 4) Snippet similarity-weighted point-wise reconstruction:

With the learnt snippet-wise similarities, we can now perform a better reconstruction of the  $i$ -th snippet back in the point-wise representation space  $\mathcal{P}$  by taking *similarity-weighted* aggregation of the point-wise representations:

$$\hat{\mathbf{p}}_i = \sum_{\mathbf{s}' \in \mathcal{S} \setminus \{\mathbf{s}_i\}} \frac{\exp(D_{\mathbf{s}_i, \mathbf{s}'}/\tau)}{\sum_{\mathbf{s}'' \in \mathcal{S} \setminus \{\mathbf{s}_i\}} \exp(D_{\mathbf{s}_i, \mathbf{s}''}/\tau)} \mathbf{p}' \quad (4)$$

where,  $\mathbf{p}'$  is a point-wise representation,  $\mathbf{s}'$  is its snippet-wise representation, and  $\hat{\mathbf{p}}_i \in \mathbb{R}^{T \times d_f}$  is the reconstructed point-wise representation for the original snippet  $\mathbf{x}_i \in \mathbb{R}^{T \times C}$ .

Unlike a simple averaging-based reconstruction that assigns equal weights to all representations, including unrelated ones, our similarity-weighted approach enables the model to focus on similarity associations between the masked and original snippet pairs, or even other relevant snippets, while suppressing the noise from dissimilar snippets. Lastly, the reconstructed point-wise representations  $\{\hat{\mathbf{p}}_i\}_{i=1}^N$  are fed into the decoder  $d(\cdot)$  to obtain the reconstructed snippets:

$$\{\hat{\mathbf{x}}_i\}_{i=1}^N = d\left(\{\hat{\mathbf{p}}_i\}_{i=1}^N\right) \quad (5)$$

where,  $\hat{\mathbf{x}}_i \in \mathbb{R}^{T \times C}$  is the reconstruction of the original snippet  $\mathbf{x}_i \in \mathbb{R}^{T \times C}$ . The decoder is just a simple MLP layer. The reconstruction loss  $\mathcal{L}_r$  is formalized as:

$$\mathcal{L}_r = \sum_{i=1}^N \|\mathbf{x}_i - \hat{\mathbf{x}}_i\|_2^2 \quad (6)$$

The overall training loss to be minimized for our pre-training task of similarity-weighted masked reconstruction is thus

$$\mathcal{L}_{pretrain} = \mathcal{L}_r + \beta \mathcal{L}_c \quad (7)$$

where, the weight  $\beta$  is automatically tuned based on the homoscedastic uncertainty of each loss term [43]. Incorporating both losses enables our encoder to capture richer data representations—the reconstruction loss aids in learning fine-grained temporal patterns within each snippet, while the contrastive loss promotes learning of high-level associative relationships among the fragmented snippets.

TABLE II  
IMPACT OF PRE-TRAINING DATA ON CAPACITY ESTIMATION PERFORMANCE, QUANTIFIED BY RMSE (LOWER IS BETTER)

Setting	Fine-tuning/ Test data distribution	Pre-training data	
		EVM1D1	EVM1D1
In-distribution	EVM1D1	1.852±0.339	<b>1.723±0.308</b>
Out-of-distribution	EVM1D2	2.627±2.504	<b>1.388±0.252</b>
	EVM1D3	1.469±0.310	<b>1.296±0.187</b>

### B. Supervised fine-tuning for capacity estimation

Once pre-training is complete, the pre-trained encoder  $f(\cdot)$  can be leveraged for the capacity estimation task by combining it with a new regression head  $g(\cdot)$  to estimate capacity  $y_i$  of charging snippet  $\mathbf{x}_i$ . The regression head is just a single fully connected linear layer, ensuring that accurate capacity estimation primarily depends on the effectiveness of the encoder. During supervised fine-tuning, only a small amount of labeled data  $\{\mathbf{x}_i, y_i\}_{i=1}^{\bar{N}}$  with  $\bar{N} \ll N$  is needed to train the capacity estimation model  $g(f(\cdot))$ , supervised by the minimization of the squared error:

$$\mathcal{L}_{finetune} = \sum_{i=1}^{\bar{N}} \|y_i - \hat{y}_i\|_2^2 \quad (8)$$

## IV. EXPERIMENTAL RESULTS AND DISCUSSION

The model's generalizability is evaluated under three highly challenging out-of-distribution scenarios: (i) adaptability to age-induced distribution shifts across EV lifetime, (ii) transferability across different EV manufacturers, and (iii) robustness to novel test patterns unseen in the limited labeled fine-tuning data. This section discusses the capacity estimation performance and provides insights into the model components driving the performance.

### A. Overview of unlabeled pre-training data and labeled fine-tuning data

Each charging snippet contains basic battery monitoring variables, such as charging current, voltage, temperature, and is stored as a multivariate time series of length 128. Recalling that only a subset of charging snippets in the dataset have capacity labels, we briefly highlight the differences between the labeled and unlabeled snippets in the last two subplots of Fig. 4, focusing on the charging current patterns. Labeled snippets mainly consist of slow-charging patterns, while unlabeled snippets contain a significantly diverse range of charging patterns, including higher fast-charging currents.

For self-supervised pre-training, we only use charging snippets from Distribution 1. Within Distribution 1, we generate two variants for the pre-training data: (i) EVM1D1, which contains all charging snippets, including unlabeled fast-charging snippets, and (ii) EVM1D1, which only contains the initially labeled slow-charging snippets, now used without labels. These variants enable us to assess how harnessing the more diverse unlabeled snippets impacts the downstream capacity estimation performance. For the supervised fine-tuning following pre-training, labeled snippets from any of

TABLE III  
COMPARISON OF CAPACITY ESTIMATION PERFORMANCE AGAINST STATE-OF-THE-ART PRE-TRAINING FRAMEWORKS FOR TIME SERIES

Pre-training data	Fine-tuning/ Test data	Ours		PITS [37] (ICLR'24)		SimMTM [38] (NeurIPS'23)		TST [39] (SIGKDD'21)		TSLANet [40] (ICML'24)	
		RMSE	MAPE (%)	RMSE	MAPE (%)	RMSE	MAPE (%)	RMSE	MAPE (%)	RMSE	MAPE (%)
EVM1 $\tilde{D}$ 1	EVM1D1	<b>1.396</b> $\pm$ 0.171	<b>2.640</b> $\pm$ 0.421	1.555 $\pm$ 0.251	2.992 $\pm$ 0.547	1.560 $\pm$ 0.386	3.051 $\pm$ 0.855	3.992 $\pm$ 2.326	7.698 $\pm$ 4.402	2.049 $\pm$ 1.643	4.181 $\pm$ 3.772
	EVM1D2	<b>1.278</b> $\pm$ 0.175	<b>2.505</b> $\pm$ 0.389	1.452 $\pm$ 0.255	2.710 $\pm$ 0.456	1.848 $\pm$ 0.659	3.994 $\pm$ 1.668	2.553 $\pm$ 0.658	5.130 $\pm$ 1.351	1.989 $\pm$ 0.921	4.119 $\pm$ 2.100
	EVM1D3	<b>1.156</b> $\pm$ 0.085	<b>2.381</b> $\pm$ 0.154	1.567 $\pm$ 0.592	2.818 $\pm$ 0.580	1.682 $\pm$ 0.645	3.655 $\pm$ 1.572	3.297 $\pm$ 0.934	6.973 $\pm$ 2.106	2.524 $\pm$ 1.965	4.918 $\pm$ 4.907

TABLE IV  
COMPARISON OF CAPACITY ESTIMATION PERFORMANCE WHEN PRE-TRAINING AND FINE-TUNING ON DIFFERENT MANUFACTURERS (EVM3  $\rightarrow$  EVM1)

Pre-training data	Fine-tuning/ Test data	Ours		PITS [37] (ICLR'24)		SimMTM [38] (NeurIPS'23)		TST [39] (SIGKDD'21)		TSLANet [40] (ICML'24)	
		RMSE	MAPE (%)	RMSE	MAPE (%)	RMSE	MAPE (%)	RMSE	MAPE (%)	RMSE	MAPE (%)
EVM3 $\tilde{D}$ 1	EVM1D1	<b>1.402</b> $\pm$ 0.239	<b>2.671</b> $\pm$ 0.561	1.566 $\pm$ 0.286	3.036 $\pm$ 0.620	1.613 $\pm$ 0.615	3.217 $\pm$ 1.433	2.899 $\pm$ 0.975	5.455 $\pm$ 1.849	3.663 $\pm$ 2.177	8.001 $\pm$ 5.471
	EVM1D2	<b>1.344</b> $\pm$ 0.173	2.625 $\pm$ 0.355	1.365 $\pm$ 0.165	<b>2.613</b> $\pm$ 0.325	1.903 $\pm$ 0.352	4.084 $\pm$ 0.970	2.788 $\pm$ 0.500	5.477 $\pm$ 1.294	4.185 $\pm$ 1.590	8.929 $\pm$ 3.600
	EVM1D3	<b>1.206</b> $\pm$ 0.159	<b>2.429</b> $\pm$ 0.293	1.772 $\pm$ 0.833	3.124 $\pm$ 0.824	1.651 $\pm$ 0.518	3.557 $\pm$ 1.339	2.906 $\pm$ 0.649	5.954 $\pm$ 1.210	3.261 $\pm$ 1.540	7.247 $\pm$ 3.945

the Distributions 1 through 3 can be used to train a capacity estimation model optimized for the target distribution. However, unlike prior studies [9], [32], [33], we utilize only 10% labeled data to better reflect the real-world scarcity of labeled data. Details are provided in Table A.1.

### B. Impact of harnessing unlabeled data

The pre-trained encoder’s generalizability depends on both the pre-training data quality and the effectiveness of the pre-training framework’s design. Before delving into the design, we examine the impact of harnessing the unlabeled data for pre-training. We consider two versions of pre-training data, EVM1 $\tilde{D}$ 1 and EVM1D1, as defined earlier in Section IV-A. We assess the pre-trained encoder’s generalizability through its fine-tuning performance on out-of-distribution capacity estimation scenarios, where clear distribution shifts exist between the target distribution (e.g., Distribution 2 or 3) and the pre-training data from Distribution 1 (recall Fig. 2b).

Table II compares the capacity estimation performance of our encoder pre-trained on EVM1D1 and EVM1 $\tilde{D}$ 1, respectively. Pre-training on EVM1 $\tilde{D}$ 1 consistently outperforms EVM1D1 across both in-distribution and out-of-distribution test settings, as evidenced by its lower average root mean square errors (RMSE). This outperformance is especially pronounced in out-of-distribution settings, highlighting the importance of leveraging richer unlabeled charging data for developing a generalizable pre-trained encoder that can withstand data distribution shifts. Even more remarkably, harnessing the unlabeled data in EVM1 $\tilde{D}$ 1 actually yields *long-term improvements* to capacity estimation performance, as seen from the progressively decreasing RMSEs for the later-stage distributions, EVM1D2 and EVM1D3. This benefit stems from the encoder’s ability to uncover critical dependencies affecting battery capacity from the unlabeled fast charging operations, which are known to accelerate capacity degradation [15].

### C. Adaptability to age-induced distribution shifts

Next, we evaluate the effectiveness of our pre-training design by benchmarking our capacity estimation performance

against several state-of-the-art time series pre-training frameworks [37]–[40]. These frameworks have demonstrated strong performance across a wide range of domains, including healthcare and IoT. However, they have only been validated on benchmark datasets, and their ability to generalize to more challenging, privacy-friendly field data under realistic data distribution shifts has yet to be investigated. In addition to RMSE, we also report the mean absolute percentage error (MAPE) as a scale-independent measure of relative error.

All models are pre-trained only on EVM1 $\tilde{D}$ 1, and then fine-tuned on different target distributions (EVM1D1 to EVM1D3) across the EV lifetime. Table III compares the fine-tuned capacity estimation performance of our model against state-of-the-art baselines, PITS [37], SimMTM [38], TST [39], and TSLANet [40]. Not only does our model achieve the lowest RMSE across all models for both in-distribution settings (EVM1D1) and out-of-distribution settings (EVM1D2 and EVM1D3), it is also the only model to maintain a robust capacity estimation performance throughout the distribution shifts from EVM1D1 to EVM1D3, as demonstrated by its progressively decreasing RMSE. This is a highly non-trivial achievement for learning from privacy-friendly field data, especially considering the mixed and underwhelming performance delivered by the state-of-the-art baselines. In fact, even on EVM1D3, the distribution with the largest shift from the pretraining data, our model achieves a 26.2% lower RMSE than the best-performing baseline, PITS.

The suboptimal performance of the baseline pre-training frameworks may be attributed to their masked modeling design, which lacks consideration for more complex time series in field applications. For instance, TST and SimMTM rely on parameter-heavy transformer architectures not inherently suited for time series representation learning [40], while TSLANet and PITS require cumbersome data transformations like patchifying time series and Fourier transforms, which risk losing granular temporal information.

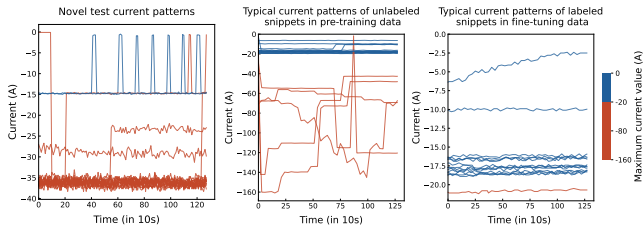


Fig. 4. Comparison of some randomly sampled current patterns from the novel test data with typical patterns observed in labeled and unlabeled snippets.

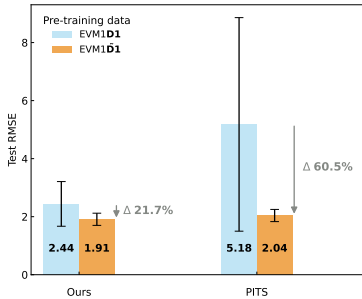


Fig. 5. Inference performance on novel test patterns beyond fine-tuning data.

#### D. Transferability across different EV manufacturers

We further evaluate the generalizability of our pre-training framework in an even more demanding transfer learning setting, where the pre-training and fine-tuning data come from two different manufacturers. For the pre-training data, we use manufacturer EVM3, which has the smallest number of charging records among the three manufacturers. The number of charging snippets now available for pre-training is less than half of that from manufacturer EVM1 (see Table A.1), which allows us to also assess the transferability of our pre-training framework across manufacturers with significantly smaller pre-training data. Due to the smaller dataset, the mileage distribution of the EVM3 charging snippets is mostly from Distribution 1, which we denote as EVM3 $\tilde{D}1$  to differentiate the manufacturer. The fine-tuning and test capacity estimation continue to be done on EVM1 $\tilde{D}1$  to EVM1 $\tilde{D}3$  from manufacturer EVM1, as before.

Table IV presents the capacity estimation results for this EVM3-to-EVM1 transfer learning setting. Even when pre-trained on a smaller dataset from a different manufacturer, our model achieves robust capacity estimation on the target distributions from EVM1, surpassing all baselines in RMSE. Although MAPE is marginally higher than PITS on EVM1 $\tilde{D}2$  (2.625% vs. 2.613%), this one-off and negligible difference is likely due to data-specific variability rather than any methodological limitation. Crucially, on the most domain-shifted distribution, EVM1 $\tilde{D}3$ —affected by both manufacturer-related and age-induced distribution shifts—our model experiences only a 4.3% performance drop compared to the previous setting of pre-training with same manufacturer. Moreover, it still achieves a 31.9% lower RMSE than PITS, the previously best-performing baseline in Table III.

TABLE V  
ABLATION STUDY

Loss components	Pre-train data	Recon. error during pre-training <sup>1</sup>	Fine-tune data	Capacity estimation error
$\mathcal{L}_r$ only	EVM1 $\tilde{D}1$	0.0439 $\pm$ 0.0025	EVM1 $\tilde{D}1$	1.435 $\pm$ 0.395
	EVM1 $\tilde{D}2$		1.317 $\pm$ 0.297	
	EVM1 $\tilde{D}3$		1.168 $\pm$ 0.110	
$\mathcal{L}_c + \mathcal{L}_r$	EVM1 $\tilde{D}1$	0.0273 $\pm$ 0.0044	EVM1 $\tilde{D}1$	1.396 $\pm$ 0.171
	EVM1 $\tilde{D}2$		1.278 $\pm$ 0.175	
	EVM1 $\tilde{D}3$		1.156 $\pm$ 0.085	

<sup>1</sup> Reconstruction error is reported as mean squared error, while capacity estimation error is reported as root mean squared error.

#### E. Robustness to novel test patterns beyond fine-tuning data

We complete our evaluation of the pre-trained encoder’s generalizability by assessing the direct inference performance of our model (without further fine-tuning) on novel test charging patterns unseen in the limited fine-tuning data. To recap, labeled charging snippets available for fine-tuning are mainly from regular, slow-charging scenarios with current values below 20 A. However, a few rare EVs of the remaining manufacturer, EVM2, have labeled snippets with current values up to 40 A—significantly higher than typical labeled snippets, but still lower than the fast-charging currents in unlabeled snippets (see Fig. 4). These novel labeled charging data serve as an insightful test case for evaluating the model’s inference performance on rare yet operationally plausible patterns beyond the limited fine-tuning data.

As the mileage distribution of these test snippets is below 100,000 km and thus falls within Distribution 1, we select the model fine-tuned on EVM1 $\tilde{D}1$  for the inference. For pre-training, we revisit the two variants of pre-training data from Distribution 1, EVM1 $\tilde{D}1$  and EVM1 $\tilde{D}1$ , to also distinguish the impact of the pre-training data versus methodology design on inference performance. Fig. 5 compares our model’s direct inference performance on these novel test data (without further fine-tuning) against the strongest baseline from earlier experiments, PITS. Despite the added complexity of the test data, our model remains robust, consistently achieving lower RMSE than PITS, regardless of whether it was pre-trained on the more diverse EVM1 $\tilde{D}1$  or the limited EVM1 $\tilde{D}1$ . This robustness is a strong testament to the effectiveness of our pre-training methodology, rather than just a consequence of the scale and quality of the pre-training data. In comparison, not only is PITS’s inference performance on novel test patterns worse, but it is also more dependent on the pre-training data quality—as evidenced by the substantial data-driven performance gain ( $\Delta 60.5\%$ ) needed to even achieve a comparable performance (RMSE = 2.04) to our model (RMSE = 1.91).

#### F. Ablation study and sensitivity analysis

For the ablation study, we investigate the impact of both the contrastive loss component for similarity learning and the choice of encoder architecture. As shown in Table V, incorporating similarity learning via contrastive loss not only reduces masked reconstruction error during pre-training, but

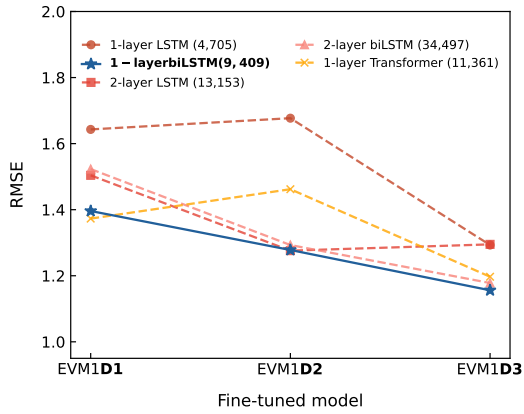


Fig. 6. Performance of different encoder architectures (and parameter count).

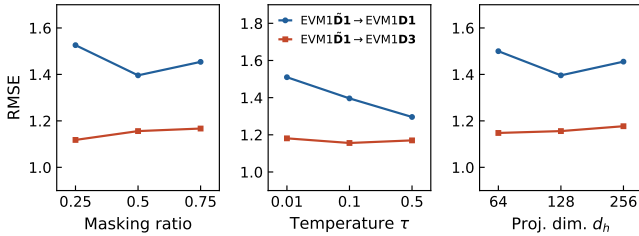


Fig. 7. Sensitivity analysis of key hyperparameters on two representative fine-tuning settings: in-distribution EVM1D1 and out-of-distribution EVM1D3.

also improves the accuracy and stability (lower standard deviation) of downstream capacity estimation.

Fig. 6 presents the downstream capacity estimation performance and model parameter sizes of several candidate encoder architectures. Compared to transformers or deeper LSTMs, the chosen 1-layer biLSTM encoder achieves the best balance of capacity estimation accuracy, parameter efficiency, and generalization across different fine-tuning scenarios. Its effectiveness stems from the ability to capture temporal dependencies in both past and future directions, which is especially valuable given the limited temporal context in fragmented charging snippets.

We also analyze the model’s sensitivity to key hyperparameters such as masking ratio, projector dimension size  $d_h$ , and contrastive learning temperature constant  $\tau$ . Fig. 7 reports the capacity estimation performance on two representative fine-tuning settings: in-distribution EVM1D1 and out-of-distribution EVM1D3. A masking ratio of 0.5 strikes a good balance between reconstruction difficulty and effective representation learning, yielding strong capacity estimation performance in both in-distribution and out-of-distribution settings. Increasing the ratio beyond 0.5 to 0.75 tends to degrade performance, likely due to the greater complexity of reconstructing heavily masked field data. Next, the projector dimension  $d_h$  governs the expressiveness of the snippet-wise representation space used for computing contrastive similarity. Strong capacity estimation performance is achieved in both in-distribution and out-of-distribution settings with  $d_h = 128$ . Increasing  $d_h$  beyond 128 to 256 leads to performance deterior-

ation, likely due to overparameterization of the projector relative to the input features. Finally, the temperature parameter  $\tau$  in the contrastive loss controls the sharpness of the similarity distribution over snippet-wise representation pairs. If  $\tau$  is too low (e.g., 0.01 as shown in Fig. 7), similarity learning may be constrained to only the most similar pairs, such as masked versions of the same snippet. If too high, the learnt similarities may not be meaningfully discriminative. Reasonably ranged values like 0.1 and 0.5 yield stronger capacity estimation, with  $\tau = 0.1$  providing a favorable balance across both in-distribution and out-of-distribution settings.

### G. Interpretability analysis

We investigate the internal learning mechanism that underpins the rich representation learning and generalizability of our framework. The key feature of our *snippet similarity-weighted masked reconstruction* is its ability to capture both fine-grained temporal patterns within a snippet and high-level similarity associations across snippets. We begin with a high-level examination of the learnt similarity weights used during masked reconstruction. Due to the large size of the similarity matrix, Fig. 8a only presents a subset of snippets and their learnt similarity weights to other snippets, including both the original and masked versions. Each row represents the similarity weights contributing to the reconstruction of a single battery monitoring time series variable (e.g., current) in a given snippet. As expected, the highest weights typically correspond to the masked version of the same snippet (seen as offset diagonals). However, the presence of large similarity weights at some non-offset positions indicates that the model also leverages similarities from other relevant variables and snippets to improve reconstruction.

Figs. 8b–d offer a granular view of the reconstruction process for individual battery time series variables from selected snippets. The radial plots (left) highlight the battery variables and snippets with the highest similarity weights contributing to the target variable’s reconstruction. The reconstruction plots (right) depict the corresponding reconstruction performance for the target variable. As evident from these plots, reconstructing field data is particularly challenging due to the noisy and erratic nature of signals in field applications. Thus, a successful reconstruction relies on effective similarity learning from appropriate snippets—whether from the masked version of the target snippet (Fig. 8b), from other correlated variables within the same snippet (Fig. 8c), or even from entirely different but contextually relevant snippets (Fig. 8d).

### H. Computational complexity analysis

The main source of computational complexity in our pre-training method is the pairwise similarity computation. The batched similarity matrix  $\mathbf{D}$  has size  $2M \times 2M$ , where  $M = b \cdot C$ , with  $b$  as the batch size and  $C$ , to recap, the number of battery monitoring variables.

Therefore, the memory complexity of storing the similarity matrix is  $\mathcal{O}(b^2C^2)$ , and the time complexity of the similarity computation is  $\mathcal{O}(b^2C^3)$ . As a large batch size can increase

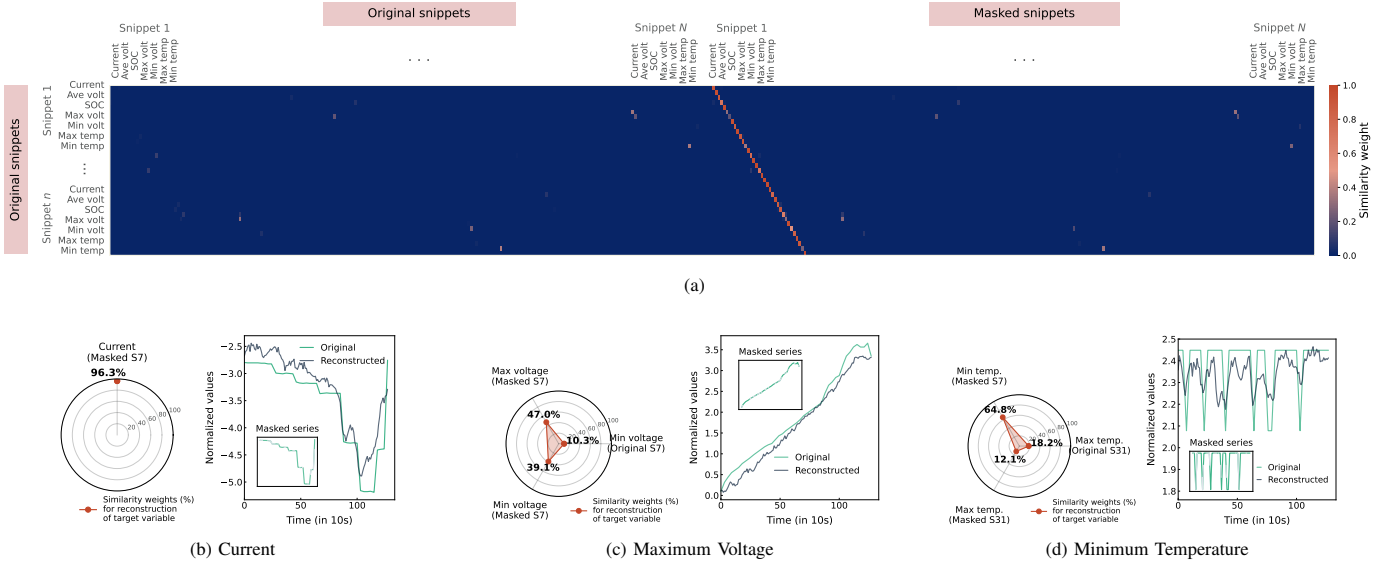


Fig. 8. Understanding the internal mechanism of our model which enables the rich representation learning of both granular temporal patterns within a snippet and high-level similarity associations among different snippets. Taking a high-level view of the similarity matrix, (a) presents a subsample of snippets along the rows and their learned similarity weights to all other snippets along the columns, including both the original and masked versions. (b) to (d) provide a granular view into the similarity-weighted reconstruction process of individual battery charging variables, where S7 denotes Snippet 7, and so on.

training time, we adopt  $b = 32$  to balance computational efficiency and representational learning adequacy. Moreover, the number of input feature variables in the privacy-preserving charging data is inherently low, with  $C = 7$ . Consequently, the similarity matrix computation takes approximately just  $3.03 \times 10^{-4}$  seconds per batch-per epoch, with a peak memory usage of 0.99 MB on a NVIDIA RTX 3070 GPU.

In this work, the scale of the similarity matrix computation is manageable, as our pre-training method is designed to effectively leverage less feature-rich, privacy-preserving data. However, optimizations such as top- $K$  neighbor truncation [44] or a modified memory bank [45] could also be explored in future iterations.

### I. Implementation details

We summarize the key implementation details here. A 70%–10%–20% split of vehicles is adopted for pre-training, validation, and testing. For fine-tuning, only 10% of vehicles within the pre-training split are used. Snippet-level normalization is performed using a range-adjusted z-score normalization, as recommended for this dataset in [41].

For time series masking, we apply geometric masking [39] with a masking ratio of 0.5, randomly replacing temporal subsequences with zeros. For contrastive learning,  $\tau = 0.1$ . Batch size is set to 32. The model architecture consists of a single-layer biLSTM encoder with  $d_f = 32$ , an MLP projector with  $d_h = 128$ , and a linear regression head with output dimension 1.

Model training is performed with the Adam optimizer. The learning rate is scheduled with a maximum initial value of 0.01. Pre-training is conducted for 50 epochs, averaging around 83.06 seconds per epoch. Fine-tuning is conducted for 200 epochs with early stopping, averaging around 0.86

seconds per epoch. The inference time is negligible, averaging approximately  $3.80 \times 10^{-5}$  seconds per test snippet.

Experiments were conducted on a NVIDIA RTX 3070 (8GB) GPU. Each experiment was repeated with 5 different random seeds to ensure robustness of model performance. The average model performance and standard deviation are reported. For benchmark models, we follow hyperparameters recommended in the respective papers and official code, applying additional tuning as needed for our dataset.

## V. CONCLUSION

To realize the potential of DL for practical EV adoption, generalizable models capable of adapting to real-world distribution shifts are needed. However, no prior studies have delved deeply into model generalizability and rigorously tested their capacity estimation models on realistic out-of-distribution scenarios. Compounded with the challenges of privacy and data labeling costs, there is a need to rethink the reliance on extensive, well-labeled training data to achieve model generalizability. In this work, we developed a first-of-its-kind capacity estimation model based on self-supervised learning, designed to learn rich, generalizable representations even from less feature-rich and fragmented privacy-friendly data. With our snippet-wise contrastive learning and subsequent similarity-weighted masked reconstruction, we can learn rich representations of both granular charging patterns within individual snippets and high-level associative relationships across different snippets. Bolstered by the rich representation learning, our capacity estimation framework achieved new state-of-the-art performance across multiple out-of-distribution settings, with only 10% labeled fine-tuning data.

We encourage the research community to build on this new research direction and prioritize the development of general-

izable, future-ready prognostics models that are labeled data-efficient and privacy-friendly. Another future area of interest is integrating difficulty-aware uncertainty quantification into the framework to provide prediction confidence as an added reliability measure, particularly under extreme distribution shifts. Beyond battery capacity estimation, as our pre-training framework is generalizable and domain-agnostic, it can also be adapted to other applications where learning from fragmented, privacy-protected sensor data is crucial (e.g., autonomous vehicles, smart manufacturing).

## APPENDIX A

TABLE A.1

OVERVIEW OF DATA SPLITS USED FOR PRE-TRAINING AND FINE-TUNING

Task	Data distribution	Train	Validation	Test
		Number of vehicles <sup>1</sup>	Number of snippets <sup>2</sup>	
Pre-training	EVM1D1	23 / 54,234	3 / 6,007	NA
	EVM1D1	23 / 69,354	3 / 7,598	NA
	EVM3D1	5 / 28,937	1 / 7,350	NA
Fine-tuning	EVM1D1	2 / 4,663	3 / 6,007	6 / 13,584
	EVM1D2	2 / 3,472	3 / 6,388	7 / 14,170
	EVM1D3	2 / 4,582	3 / 4,553	7 / 11,333

<sup>1</sup> We adopt a 70%–10%–20% split of vehicles for pre-training, validation, and testing. For fine-tuning, only 10% of vehicles within the pre-training split (i.e., two vehicles' worth of data) are used. Each vehicle is uniquely assigned to exactly one split, ensuring that the train–validation–test splits are strictly disjoint with no cross-split information leakage.

<sup>2</sup> For brevity, we report only the average number of vehicles and charging snippets across five randomly generated train–validation–test splits used in the experiments.

## REFERENCES

- [1] S. Li, P. Zhao, C. Gu, J. Li, S. Cheng, and M. Xu, "Battery protective electric vehicle charging management in renewable energy system," *IEEE Transactions on Industrial Informatics*, vol. 19, no. 2, pp. 1312–1321, 2022.
- [2] F. Javadnejad, M. Jahanbakh, C. A. Pinto, and A. Saeidi, "Analyzing incentives and barriers to electric vehicle adoption in the united states," *Environment Systems and Decisions*, pp. 1–32, 2023.
- [3] V. Sulzer, P. Mohtat, A. Aitio, S. Lee, Y. T. Yeh, F. Steinbacher, M. U. Khan, J. W. Lee, J. B. Siegel, A. G. Stefanopoulou *et al.*, "The challenge and opportunity of battery lifetime prediction from field data," *Joule*, vol. 5, no. 8, pp. 1934–1955, 2021.
- [4] D. Zhang, Z. Wang, P. Liu, C. She, Q. Wang, L. Zhou, and Z. Qin, "A multi-step fast charging-based battery capacity estimation framework of real-world electric vehicles," *Energy*, vol. 294, p. 130773, 2024.
- [5] Q. Wang, Z. Wang, L. Zhang, P. Liu, and L. Zhou, "A battery capacity estimation framework combining hybrid deep neural network and regional capacity calculation based on real-world operating data," *IEEE Transactions on Industrial Electronics*, vol. 70, no. 8, pp. 8499–8508, 2022.
- [6] Y. Wang, Y. Yu, K. Sun, P. Lei, Y. Zhang, E. Zio, A. Xia, and Y. Li, "Rmgpt: A foundation model with generative pre-trained transformer for fault diagnosis and prognosis in rotating machinery," *IEEE Internet of Things Journal*, pp. 1–1, 2025.
- [7] Y. Wang, P. Lei, J. Song, Y. Hao, T. Chen, Y. Zhang, L. Jia, Y. Li, and Z. Wei, "Ifformer: Bridging time series and natural language for multi-modal qa with large-scale multitask dataset," in *Proceedings of the 42nd International Conference on Machine Learning (ICML)*, Jul 2025.
- [8] G. Dos Reis, C. Strange, M. Yadav, and S. Li, "Lithium-ion battery data and where to find it," *Energy and AI*, vol. 5, p. 100081, 2021.
- [9] Y. Wang, L. Shen, Y. Zhang, Y. Li, R. Zhang, and Y. Yang, "Self-supervised health representation decomposition based on contrast learning," *Reliability Engineering & System Safety*, vol. 239, p. 109455, 2023.
- [10] J. Sun, G. Xu, H. Li, T. Zhang, C. Wu, X. Yang, and R. H. Deng, "Sanitizable cross-domain access control with policy-driven dynamic authorization," *IEEE Transactions on Dependable and Secure Computing*, 2025.
- [11] J. Sun, C. Wu, S. Mumtaz, J. Tao, M. Cao, M. Wang, and V. Frascolla, "An efficient privacy-aware split learning framework for satellite communications," *IEEE Journal on Selected Areas in Communications*, vol. 42, no. 12, pp. 3355–3365, 2024.
- [12] L. You, Z. Guo, C. Yuen, C. Y.-C. Chen, Y. Zhang, and H. V. Poor, "A framework reforming personalized internet of things by federated meta-learning," *Nature Communications*, vol. 16, no. 1, p. 3739, 2025.
- [13] O. J. Gstrein, N. Haleem, and A. Zwitter, "General-purpose AI regulation and the European Union AI Act," *Internet Policy Review*, vol. 13, no. 3, pp. 1–26, 2024.
- [14] U. Ahmad, M. Han, A. Jolfaei, S. Jabbar, M. Ibrar, A. Erbad, H. H. Song, and Y. Alkhrijah, "A comprehensive survey and tutorial on smart vehicles: Emerging technologies, security issues, and solutions using machine learning," *IEEE Transactions on Intelligent Transportation Systems*, vol. 25, no. 11, pp. 15 314–15 341, 2024.
- [15] R. Zhou, R. Zhu, C.-G. Huang, and W. Peng, "State of health estimation for fast-charging lithium-ion battery based on incremental capacity analysis," *Journal of Energy Storage*, vol. 51, p. 104560, 2022.
- [16] J. Lu, R. Xiong, J. Tian, C. Wang, and F. Sun, "Deep learning to estimate lithium-ion battery state of health without additional degradation experiments," *Nature Communications*, vol. 14, no. 1, p. 2760, 2023.
- [17] Y. Wang, P. Lei, X. Wang, L. Jiang, L. Xuan, W. Cheng, H. Zhao, and Y. Li, "Leveraging large self-supervised time-series models for transferable diagnosis in cross-aircraft type bleed air system," *Advanced Engineering Informatics*, vol. 65, p. 103275, 2025.
- [18] Y. Wang, Y. Li, Y. Zhang, J. Lei, Y. Yu, T. Zhang, Y. Yang, and H. Zhao, "Incorporating prior knowledge into self-supervised representation learning for long phm signal," *Reliability Engineering & System Safety*, vol. 241, p. 109602, 2024.
- [19] C. She, Z. Wang, F. Sun, P. Liu, and L. Zhang, "Battery aging assessment for real-world electric buses based on incremental capacity analysis and radial basis function neural network," *IEEE Transactions on Industrial Informatics*, vol. 16, no. 5, pp. 3345–3354, 2019.
- [20] L. Song, K. Zhang, T. Liang, X. Han, and Y. Zhang, "Intelligent state of health estimation for lithium-ion battery pack based on big data analysis," *Journal of Energy Storage*, vol. 32, p. 101836, 2020.
- [21] J. Hong, Z. Wang, and Y. Yao, "Fault prognosis of battery system based on accurate voltage abnormality prognosis using long short-term memory neural networks," *Applied Energy*, vol. 251, p. 113381, 2019.
- [22] J. Hong, Z. Wang, W. Chen, L. Wang, P. Lin, and C. Qu, "Online accurate state of health estimation for battery systems on real-world electric vehicles with variable driving conditions considered," *Journal of Cleaner Production*, vol. 294, p. 125814, 2021.
- [23] Z. Wang, C. Song, L. Zhang, Y. Zhao, P. Liu, and D. G. Dorrell, "A data-driven method for battery charging capacity abnormality diagnosis in electric vehicle applications," *IEEE Transactions on Transportation Electrification*, vol. 8, no. 1, pp. 990–999, 2021.
- [24] Z. Deng, L. Xu, H. Liu, X. Hu, Z. Duan, and Y. Xu, "Prognostics of battery capacity based on charging data and data-driven methods for on-road vehicles," *Applied Energy*, vol. 339, p. 120954, 2023.
- [25] Y. Lu, D. Guo, G. Xiong, Y. Wei, J. Zhang, Y. Wang, and M. Ouyang, "Towards real-world state of health estimation: Part 2, system level method using electric vehicle field data," *eTransportation*, vol. 22, p. 100361, 2024.
- [26] C. She, L. Zhang, Z. Wang, F. Sun, P. Liu, and C. Song, "Battery state-of-health estimation based on incremental capacity analysis method: Synthesizing from cell-level test to real-world application," *IEEE Journal of Emerging and Selected Topics in Power Electronics*, vol. 11, no. 1, pp. 214–223, 2021.
- [27] Z. Xu, J. Wang, P. D. Lund, and Y. Zhang, "Estimation and prediction of state of health of electric vehicle batteries using discrete incremental capacity analysis based on real driving data," *Energy*, vol. 225, p. 120160, 2021.
- [28] T. Chen, S. Kornblith, K. Swersky, M. Norouzi, and G. E. Hinton, "Big self-supervised models are strong semi-supervised learners," *Advances in Neural Information Processing Systems*, vol. 33, pp. 22 243–22 255, 2020.
- [29] K. He, X. Chen, S. Xie, Y. Li, P. Dollár, and R. Girshick, "Masked autoencoders are scalable vision learners," in *Proceedings of the IEEE/CVF Conference on Computer Vision and Pattern Recognition*, 2022, pp. 16 000–16 009.
- [30] T. Chen, S. Kornblith, M. Norouzi, and G. Hinton, "A simple framework for contrastive learning of visual representations," in *Proceedings of the*

*International Conference on Machine Learning*. PMLR, 2020, pp. 1597–1607.

- [31] C. Wu, J. Sun, J. Chen, M. Alazab, Y. Liu, and Y. Xiang, “TCG-IDS: Robust network intrusion detection via temporal contrastive graph learning,” *IEEE Transactions on Information Forensics and Security*, vol. 20, pp. 1475–1486, 2025.
- [32] T. Wang, Z. Ma, S. Zou, Z. Chen, and P. Wang, “Lithium-ion battery state-of-health estimation: A self-supervised framework incorporating weak labels,” *Applied Energy*, vol. 355, p. 122332, 2024.
- [33] Y.-X. Wang, S. Zhao, S. Wang, K. Ou, and J. Zhang, “Enhanced vision-transformer integrating with semi-supervised transfer learning for state of health and remaining useful life estimation of lithium-ion batteries,” *Energy and AI*, vol. 17, p. 100405, 2024.
- [34] J. Li, J. Zhu, Z. Huang, G. Fan, and X. Zhang, “A contrastive learning battery state of health estimation method based on self-supervised aging representation,” *IFAC-PapersOnLine*, vol. 56, no. 2, pp. 6130–6135, 2023.
- [35] M. A. Hannan, D. N. How, M. H. Lipu, M. Mansor, P. J. Ker, Z. Dong, K. Sahari, S. K. Tiong, K. M. Muttaqi, T. I. Mahlia *et al.*, “Deep learning approach towards accurate state of charge estimation for lithium-ion batteries using self-supervised transformer model,” *Scientific Reports*, vol. 11, no. 1, p. 19541, 2021.
- [36] Q. Wang, M. Ye, S. Celik, Z. Deng, B. Li, D. U. Sauer, and W. Li, “Unlocking the potential of unlabeled data: Self-supervised machine learning for battery aging diagnosis with real-world field data,” *Journal of Energy Chemistry*, vol. 99, pp. 681–691, 2024.
- [37] S. Lee, T. Park, and K. Lee, “Learning to embed time series patches independently,” in *Proceedings of the International Conference on Learning Representations (ICLR)*, 2024.
- [38] J. Dong, H. Wu, H. Zhang, L. Zhang, J. Wang, and M. Long, “Simtmn: A simple pre-training framework for masked time-series modeling,” *Advances in Neural Information Processing Systems*, vol. 36, 2024.
- [39] G. Zerveas, S. Jayaraman, D. Patel, A. Bhamidipaty, and C. Eickhoff, “A transformer-based framework for multivariate time series representation learning,” in *Proceedings of the 27th ACM SIGKDD Conference on Knowledge Discovery & Data Mining*, 2021, pp. 2114–2124.
- [40] E. Eldele, M. Ragab, Z. Chen, M. Wu, and X. Li, “TSLANet: Rethinking transformers for time series representation learning,” in *Proceedings of the 41st International Conference on Machine Learning (ICML)*, 2024.
- [41] H. He, J. Zhang, Y. Wang, B. Jiang, S. Huang, C. Wang, Y. Zhang, G. Xiong, X. Han, D. Guo *et al.*, “EVBattery: A large-scale electric vehicle dataset for battery health and capacity estimation,” 2022, arXiv preprint arXiv:2201.12358, version 3.
- [42] L. Kang and H. Shen, “Electric vehicle battery energy information is enough to track you,” in *Proceedings of 19th ACM/IEEE International Conference on Information Processing in Sensor Networks (IPSN)*. IEEE, 2020, pp. 217–228.
- [43] A. Kendall, Y. Gal, and R. Cipolla, “Multi-task learning using uncertainty to weigh losses for scene geometry and semantics,” in *Proceedings of the IEEE Conference on Computer Vision and Pattern Recognition*, 2018, pp. 7482–7491.
- [44] D. Dwibedi, Y. Aytar, J. Tompson, P. Sermanet, and A. Zisserman, “With a little help from my friends: Nearest-neighbor contrastive learning of visual representations,” in *Proceedings of the IEEE/CVF International Conference on Computer Vision*, 2021, pp. 9588–9597.
- [45] A. Bulat, E. Sánchez-Lozano, and G. Tzimiropoulos, “Improving memory banks for unsupervised learning with large mini-batch, consistency and hard negative mining,” in *Proceedings of the 2021 IEEE International Conference on Acoustics, Speech and Signal Processing (ICASSP)*. IEEE, 2021, pp. 1695–1699.